



# An interpretable graph neural network for real-world satellite power system anomaly detection based on graph filtering

Yi Di <sup>a,b</sup>, Fujin Wang <sup>a,b</sup>, Zhibin Zhao <sup>a,b</sup>, Zhi Zhai <sup>a,b,\*</sup>, Xuefeng Chen <sup>a,b</sup>

<sup>a</sup> National Key Lab of Aerospace Power System and Plasma Technology, Xi'an Jiaotong University, Xi'an 710049, PR China

<sup>b</sup> School of Mechanical Engineering, Xi'an Jiaotong University, Xi'an 710049, PR China



## ARTICLE INFO

### Keywords:

Interpretability  
Anomaly detection  
Satellite power system  
Graph neural network

## ABSTRACT

Detecting anomalies in satellites holds immense importance within the aerospace industry. Many current detection methods only focus on temporal correlations and ignore spatial correlations. To take into account both temporal and spatial features, we proposed to employ Graph Neural Networks (GNN). In fact, to develop a GNN approach that is applicable to the satellite power system anomaly detection in real-world scenarios, it is imperative to take into account the specific requirements of the aerospace industry. Our analysis and research indicate that the critical factors lie in model interpretability and data characteristics. First, as model interpretability can bring trustworthiness, traceability, and guidance, it is indispensable for the application of deep learning algorithms in satellite telemetry data anomaly detection. We created a novel graph filter: Adaptive Quadratic Approximation Graph Filter (AQAGF), which is capable of both approximation ability and response time. It is transformed into a spectral graph convolution neural network that can draw the frequency response function to provide the model interpretability. Then, to address the difficulties of telemetry data characteristics: strong noise and missing data, we introduced autoencoder architecture and adversarial training strategy to further design our anomaly detection method, called Interpretable Spatial-Temporal Graph Anomaly Detection (ISTGAD) based on AQAGF, which is robust to noise and data missing. And it is able to capture temporal and spatial correlations together within a transparent working mechanism. Finally, experiments proved that our model has better anomaly detection performance than other state-of-the-art methods, and we also provide visualizations to showcase the interpretability and working mechanism of our model. Our code and data are publicly available at: <https://github.com/DiYi1999/ISTGAD>.

## 1. Introduction

Satellite anomaly detection holds immense significance within the aerospace industry, owing to the harsh, distant, and uncertain environment of space and the degradation of component properties. An investigation on 64 public satellite fault events revealed that the cumulative financial impact resulting from power system-related failures amounted to a staggering 4.4 billion dollars (Landis et al., 2006). According to the statistics of Bingxin et al. (2013), the power system is the subsystem of the satellite that experiences the most frequent faults, causing more than 50 % of the satellite anomalies. The power system serves as the heart of the satellite, and its performance is directly linked to the successful execution of the mission (Suo et al., 2020). Therefore, it is imperative for satellites to possess anomaly detection capabilities, so

that operations personnel can promptly perform power cycle the device, switch to redundant units, or change power supply strategies (Carlton et al., 2018), thereby enhancing satellite survivability.

Traditional satellite power system anomaly telemetry data detection methods, such as threshold-based and expert system-based approaches, suffer from high false alarm rates and limited ability to detect unknown anomalies (Carlton et al., 2018). Recently, to overcome these problems and achieve better performance in anomaly detection, machine learning-based methods have been popularly applied to spacecraft telemetry data anomaly detection. However, most of them cannot detect abnormal information caused by multiple correlations (Song et al., 2022). The utilization of spatial information provides a viable solution to this issue, while enhancing the performance of anomaly detection. As graph neural networks (GNNs) have demonstrated their effectiveness in

\* Corresponding author at: National Key Lab of Aerospace Power System and Plasma Technology, Xi'an Jiaotong University, Xi'an 710049, PR China.

E-mail addresses: [dy1999@stu.xjtu.edu.cn](mailto:dy1999@stu.xjtu.edu.cn) (Y. Di), [wfj1014@stu.xjtu.edu.cn](mailto:wfj1014@stu.xjtu.edu.cn) (F. Wang), [zhaozhibin@xjtu.edu.cn](mailto:zhaozhibin@xjtu.edu.cn) (Z. Zhao), [zhaizhi@xjtu.edu.cn](mailto:zhaizhi@xjtu.edu.cn) (Z. Zhai), [chenxf@xjtu.edu.cn](mailto:chenxf@xjtu.edu.cn) (X. Chen).

modeling spatial correlation (Zhou, 2020), and have been extensively used in multidimensional time series data mining tasks (Bai, 2024; He et al., 2024; Li et al., 2023). In this paper, our work for satellite power system anomaly detection will be based on GNN.

To establish a practical and effective GNN approach for real-world satellite power system anomaly detection, the crux lies in two aspects: **a) Model interpretability:** it ensures the method is trustworthy, easy for analysis and improvement, and able to support subsequent operations and maintenance. **b) Data characteristics:** the method should focus on the characteristics of satellite power system telemetry data and address the challenges in detecting anomalies within such data.

**Model interpretability:** There is a growing body of literature in many areas that recognizes the importance of interpretability of intelligent monitoring methods (Zhao et al., 2021; Jing et al., 2022; Yairi et al., 2021; Wang, 2023), which is particularly important in satellite power systems anomaly detection (Yairi et al., 2021). Some authors have made an initial exploration: Zeng et al. (Zeng et al., 2022) proposed an anomaly detection framework called CN-FA-LSTM based on the causal network (CN) and feature-attention-based (FA) long short-term memory (LSTM), which has causal relationship interpretability. We have summarized three reasons why an interpretable satellite power system anomaly detection method is required:

- (i) Trustworthiness: Trustworthiness is crucial for satellites due to the significant expenses involved in their launch and operation. Although deep learning methods have achieved high precision, these methods are still not to be trusted by humans due to the lack of underlying mathematical and theoretical foundations. With no guarantee that they will still reproduce their excellent performance when actually deployed, humans cannot entrust these black-box models with tasks that have such a huge failure cost.
- (ii) Traceability: In fact, we hope that anomaly detection will also support overall health management, further answering questions such as “Why is it considered anomalous?”, “How serious is it?”, “Where did the anomaly occur?” and so on (Yairi et al., 2021). The understandability of anomaly detection results and their processes will bring traceability. It not only helps to understand which component is anomalous (hence, to diagnose the root cause), but also speeds up the analysis process of the operation team (Nalepa et al., 2022). Additionally, the intermediate features may have practical uses, and contribute to a better understanding about possible exception types in circumstances (León-López et al., 2022).
- (iii) Guidance: An intuitive feeling is that improved interpretability often comes with a sacrifice of precision or computational efficiency. However, as a matter of fact, the optimization designs and precision improvements of “black-box” models are limited by their opacity. The research on model interpretability can help human understand the internal mechanism, which would provide guidance for model improvement and point out the direction for performance improvement (Wang et al., 2023). At the same time, interpretability can also provide an evaluation of anomaly detection methods, facilitate model selection, and provide feedback guidance on what data should be collected.

**Data characteristics:** To ensure the practicality of our approach in real-world satellite power system anomaly detection, targeted adaptations must be implemented. We summarize two characteristics of satellite power system telemetry data, which are also two difficulties in anomaly detection:

- (i) Highly noisy: Due to temporary sensor errors and the impact of complex space transmission environment, such as space particle radiation and electromagnetic interference, spacecraft telemetry data is always highly noisy (Jiang et al., 2020). To solve this problem, Wang et al. (Wang et al., 2023) viewed telemetry data as

a combination of long-term trend factor, periodic factor, short-term fluctuation factor, and auxiliary factor, and used an exponentially-weighted average (EWMA) to obtain the denoised time series. However, most researchers solve the noise problem by some pre-processing methods. For example, Xie et al. (2021) used wavelet threshold denoising, and the comparison diagram indicates that they achieved good denoising results. However, these methods always consume computational resources.

- (ii) Data missing: Due to inadequate coverage of ground receiving stations, space electromagnetic and radiation environment, limited bandwidth of communication channels, congestion of network channels, confined memory space of buffer register, components physical damage, etc., satellite telemetry data are always partly missing (Lu et al., 2019); which affects the effectiveness of anomaly detection. For example, approximately 5,000 rows of data were deleted due to large missing segments in the pre-processing of Jin et al. (2019). More than half of the satellite telemetry data are missing in (Yairi et al., 2017), and the authors used piecewise constant interpolation to fill the gaps. The reason why they did not choose a more advanced method is that the noise in the data will mislead and produce anomaly.

**Our Solution:** In this paper, we designed a new anomaly detection method called ISTGAD (Interpretable Spatial-Temporal Graph Anomaly Detection), which is based on AQAGF (Adaptive Quadratic Approximation Graph Filter). AQAGF is completely interpretable used to capture the spatial information. It can plot the frequency response function to indicate which frequency domain components AQAGF focuses on and how AQAGF expands or shrinks each frequency band. AQAGF enables ISTGAD to have a transparent working mechanism, so that it can finish interpretable anomaly detection and provide support for overall health management with high credibility. Furthermore, ISTGAD incorporates an autoencoder architecture and employs adversarial training strategies to enhance its robustness against high noise and missing data thereby ensuring its practicality in real-world anomaly detection for satellite power systems.

To summarize, the main contributions of our work are summarized as follows:

- To provide model interpretability, we proposed a novel graph filter and transformed it into a spectral graph convolution method called AQAGF, which was used to capture spatial correlations. In contrast to other graph convolution methods, AQAGF surpasses them by providing the corresponding frequency response function, thereby ensuring its ability to provide interpretability.
- To solve the challenges of data characteristics, based on AQAGF, we introduced an autoencoder architecture and an adversarial training strategy to design ISTGAD, which is effective in dealing with high noise and data missing in satellite power system telemetry data. Additionally, benefitting from AQAGF, ISTGAD has a transparent working mechanism, which can provide the O&M team (Operations and Maintenance team) with robust information assistance for subsequent cause analysis, anomaly location and so on.
- Experiments show that our method is suitable for real-world satellite power system telemetry data anomaly detection, and its performance is better than other baseline methods. The internal working mechanism of the proposed method has also been illustrated by various visualizations.

## 2. Related Work

### 2.1. Machine learning-based methods for spacecraft telemetry data anomaly detection

Sakurada and Yairi (2014) used an autoencoder with nonlinear dimensionality reduction capabilities to perform anomaly detection

tasks on real spacecraft telemetry datasets. Hundman et al. (2018) utilized LSTM (Long Short-Term Memory) for spacecraft telemetry data anomaly detection and proposed a non-parametric anomaly thresholding approach. Liu et al. (2017) proposed a segment anomaly detection strategy based on Least Squares Support Vector Machine (LS-SVM) uncertainty estimation and statistical analysis for spacecraft condition monitoring. Parisot et al. (2019) developed an Internet of Things (IoT) data analysis platform specifically for the aerospace domain, named Decision Management System for Safer Spacecrafts (DMSS). OmniAnomaly (Su et al., 2019) offered a stochastic recurrent neural network to detect anomalies, which is robust and performs well for a range of devices. Jin et al. (2022) argued that the seq2seq model is more effective in satellite power subsystem anomaly detection and proposed a seq2seq scheme based on Convolutional Neural Network (CNN). Baireddy et al. (Baireddy, et al., 2021) provided a transfer learning-based method to train a predictor model and adapted it to find telemetry channel's abnormalities. Tariq et al. (Tariq, et al., 2019) developed a hybrid approach combining a multivariate Convolutional LSTM with a Probabilistic Principal Component Analyzers for detecting potential anomalies in the KOMPSAT-2 satellite. Pang et al. (2019) combined probabilistic prediction-based methods with Markov chains to calculate the support probability for each test sequence for anomaly detection. Wu et al. (Wu et al., 2020) proposed a method based on LSTM and Ensembled One-Class Support Vector Machines to provide stable anomaly detection performance. Yang et al. (2021) proposed an attention mechanism-augmented double-layer LSTM model for spacecraft telemetry data anomaly detection. Most studies in this field have only focused on capturing temporal correlations (Wang et al., 2021). Our work aims to emphasize the importance and superiority of spatial correlation, in addition to temporal correlation, for anomaly detection in spacecraft telemetry data.

## 2.2. Spatial information capturing in spacecraft telemetry data anomaly detection

Neglecting spatial information will result in the waste of information. If the dependencies among sensor sequences can be accurately modeled, there is significant potential for enhancing both the accuracy and efficiency of anomaly detection (Bosman et al., 2017). A few studies have noted the importance of spatial correlations: Dheepadharshani et al. (2019) used Kernel Principal Component Analysis (KPCA) and Multilayer Perceptron (MLP) to capture spatial correlations, which is computationally inefficient and not powerful enough. Yu et al. (2021) used a time-scale convolutional kernel and a spatial-scale convolutional kernel to capture temporal correlations and spatial correlations, respectively, and combined them with generative adversarial network (GAN), which obtained good anomaly detection results. Pilastre et al. (2020) employed sparse representation and dictionary learning to consider the underlying correlations among parameters for spacecraft health monitoring tasks. However, these methods often involve complex calculations. The most effective way to capture spatial information is graph neural networks (GNNs), which is also the starting point for our work.

## 2.3. GNNs for time series anomaly detection

Classical graph neural networks such as GCN (Kipf and Welling, 2016), GAT (Veličković et al., 2018), and GraphSAGE (Hamilton et al., 2017) have demonstrated remarkable proficiency in capturing spatial information. Building upon these foundations, researchers across various fields have developed a variety of GNNs for time series anomaly detection. Some representative works include: CCM-CDT (Grattarola et al., 2020), MTAD-GAT (Zhao, et al., 2020), GDN (Deng and Hooi, 2021), GANF (Dai and Chen, 2022), VGCRN (Chen et al., 2022), GTA (Chen et al., 2022), MST-GAT (Ding et al., 2023), and others. Ming et al. made a detailed review (Jin, et al., 2007). However, these widely used

spatial graph convolution-based methods lack interpretability, their opaque internal mechanisms hinder practical deployment for satellite anomaly detection. Our work dedicated to addressing this problem by introducing a branch of graph signal processing: Graph Filtering.

## 3. Preliminarily

### 3.1. Temporal correlations and spatial correlations

In the research field of this study, unlike temporal correlation, which has a solid research foundation and a clear definition referring to the information contained in historical time steps, including periodicity, trends, etc., the research foundation for spatial correlation is relatively weak. But there are always complex and strong coupling relationships among the sensors of the satellite power system (Peng et al., 2016). It deserves more attention and application. Our understanding of spatial correlation is as follows: (a) Physical correlation: The most direct way for satellite power system information transmission is physical connection, physical correlation usually relying on knowledge in the circuit design field. For example, the Buck, Super-Buck, SMART, and other circuit topologies commonly used in BCR circuits establish a physical causality between their various input and output signals. (b) Logical correlation: As a complex power system with various charging and discharging strategies, power supply and distribution strategies, the satellite power system simultaneously includes data flow, control flow, and energy flow. Logical correlation relies on control processes, data flow direction, and energy exchange. For example, the explicit control logic correlation between control commands and physical measurement signals in the MSL dataset. (c) Data correlation: Unlike physical correlation, data correlation does not emphasize physical causality but refers to linear correlation, nonlinear correlation, rule correlation, and other types of correlation information manifested at the data level. For example, although there is no physical circuit connection between the X-axis solar panel voltage and the Z-axis solar panel voltage measurements, they still exhibit similar behavioral patterns and are strongly correlated at the data level.

Taking the real data of BIRDS (Cespedes et al., 2022) as an example, the fragments of the + Y solar panel of BIRDS-4 (Tsuru) satellite telemetry data on September 7, 2021 are captured for illustration, as shown in Fig. 1. During this 90 s, BIRDS-4 (Tsuru) satellite rotates and faces the sun at varying angles. It can be observed that once the voltage value reaches above 4000 mV (1200 to 1500 mV is the residual voltage generated by the panel system's Analog to Digital Converter (ADC) circuit), a corresponding current will be generated. As the product power increases, the temperature value starts to rise. Then, as the effective current can only flow for about 40 s (because a specific potential difference is required in the circuit between the panel output and the input of the DC/DC converter for the current to start flowing), the temperature also tends to decrease as the power decreases. Although there are some delays, it is clear that we can observe the interrelationship among the various sensors. They are typical spatial correlations.

### 3.2. Graph definition

The graph is a new data format, different from text, time series, and images. As shown in Fig. 2, graph has two main elements: nodes and edges. And a high-frequency graph implies that the nodes connected by edges experience drastic changes, whereas a low-frequency graph signifies that the node variations along the connections of the edges are relatively smooth. In this work, the nodes represent the sensors and the edges represent the coupling between the two sensors they connect. Specifically, an undirected graph can be represented as  $G = (O, E)$  with  $O = \{o_1, \dots, o_N\}$  is a set of nodes and  $E = \{(o_1, o_i), \dots, (o_j, o_N)\}$  is a set of edges among nodes. In fact, there are some important matrices in the operation of graph data. The adjacency matrix of  $G$  is defined as

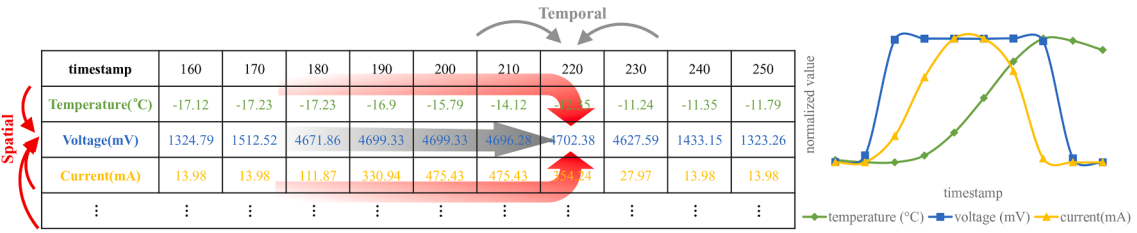


Fig. 1. Illustrative example of spatial correlations and temporal correlations.

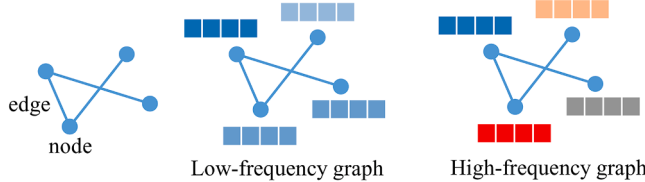


Fig. 2. A small example of graph and graph frequency.

$A \in \mathbb{R}^{N \times N}$ , where the existence of an edge  $((o_i, o_j) \in E)$  of nodes  $o_i$  and  $o_j$  is represented through  $A_{ij} = 1$ . The degree matrix is defined as  $D = \text{diag}(d_1, \dots, d_N)$ , where  $d_i = \sum_j A_{ij}$  represents the number of connected edges of the node  $o_i$ . And the Laplacian matrix is defined as  $L = D - A$ , which can be used for graph time-spectral domain conversion. Its symmetrically normalized format is  $\tilde{L} = I - D^{-1/2}AD^{-1/2}$ , where  $I$  is an identity matrix.

### 3.3. Graph filtering

The graph Fourier transform is introduced to define graph filtering in the spectral domain. In order to enhance clarity and comprehension, this paper does not differentiate between the frequency domain and spectral domain unless explicitly specified, given their similarity in theories. Denote the eigenvalue decomposition of  $\tilde{L}$  as  $\tilde{L} = U\Lambda U^T = U\text{diag}(\lambda_1, \dots, \lambda_N)U^T$ , where the  $i$ -th column of  $U$  and the  $i$ -th diagonal element of  $\Lambda$  are the  $i$ -th eigenvector and eigenvalue of  $L$ , respectively. They correspond to the  $i$ -th base and frequency of the Fourier transform, which can be used to compute the Fourier transform for a graph signal  $x$  as:  $x(\lambda_i) = \langle x, u_i \rangle = \sum_{n=1}^N x(n)u_i(n)$ . For the input observed multidimensional time series sample data, which is also the node attribute matrix  $X \in \mathbb{R}^{N \times L}$ , its graph Fourier transform  $X_f$  and inverse graph Fourier transform can be written as:  $X_f = U^T X$  and  $X = UX_f$ , respectively.

As shown in Fig. 3, based on graph Fourier transform and inverse graph Fourier transform, we can define the spectral graph filtering process as:

$$\tilde{X} = Uh(\Lambda)U^T X = U\text{diag}[h(\lambda_1), \dots, h(\lambda_N)]U^T X, \quad (1)$$

where  $h(\cdot)$  is the Frequency Response Function (FRF). Eq. (1) can be described as follows: first,  $X$  left multiplied by  $U^T$  to transform to the frequency domain, then multiplied by  $h(\Lambda)$  (frequency response matrix) to scale up or down each frequency component, accordingly, finally

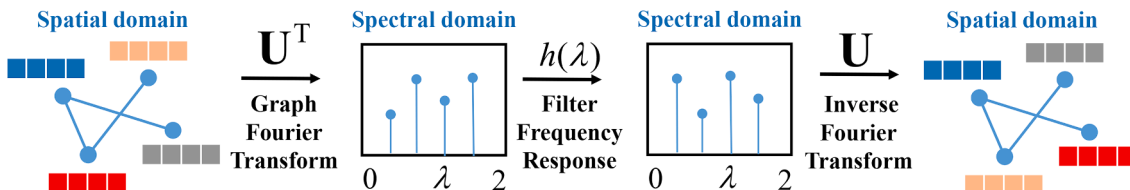


Fig. 3. Spectral graph filtering process.

multiplied by  $U$  to return to the spatial domain.

The main challenge at present lies in designing a polynomial expression to efficiently approximate various desired FRF  $h(\cdot)$  (just like shown in Fig. 2 and Fig. 4 in (He et al., 2021)). Defferrard et al. (2016) used Chebyshev polynomial of order  $k$  to approximate the FRF:

$$h(\lambda) = \sum_{k=0}^{K-1} \theta_k T_k(\tilde{\lambda}) = \sum_{k=0}^{K-1} \theta_k T_k(2\lambda/\lambda_{\max} - 1), \quad (2)$$

where  $T_k(\cdot)$  is the  $k$  order Chebyshev polynomial,  $K$  is the order of the polynomial,  $\theta_k$  are the coefficients of the polynomial, which are also learnable parameters, and  $\lambda_{\max}$  is the largest eigenvalue of  $L$ . Chien et al. (2021) proposed GPR-GNN, which used a power series-like polynomial to approximate the FRF:

$$h(\lambda) = \sum_{k=0}^K \theta_k \lambda^k = \theta_0 + \theta_1 \lambda^1 + \dots + \theta_K \lambda^K. \quad (3)$$

In 2021, He et al. (2021) proposed BernNet, which used Bernstein polynomial to approximate the FRF:

$$h(\lambda) = \sum_{k=0}^K \theta_k \frac{1}{2^k} \frac{K!}{k!(K-k)!} (2 - \lambda)^{K-k} \lambda^k. \quad (4)$$

In 2022, He et al. (2022) proposed ChebNetII, which used Chebyshev interpolation, and its FRF is defined as:

$$h(\lambda) = \frac{2}{K+1} \sum_{k=0}^K \sum_{j=0}^K \gamma_j T_k \left( \cos \left( \frac{(j+\frac{1}{2})\pi}{K+1} \right) \right) T_k \left( \frac{2\lambda - \lambda_{\max}}{\lambda_{\max}} \right). \quad (5)$$

In general, Eq. (2) has a poorer approximation ability than Eq. (3) and Eq. (4), because the illegal coefficients learned during training often lead to over-fitting (He et al., 2022). The approximation ability of Eq. (3) is also limited, when we want to approximate a more complex FRF, a very high order is required. The best approximation performance is achieved by Eq. (4) and Eq. (5), but it can be seen that both of their expressions are very complex. Both methods are expensive in time complexity, which hinders their practical deployment for satellite power system anomaly detection. Because O&M personnel have to respond to anomalies in a timely and rapid manner, which requires anomaly detection methods to control computing time. Overall, one of our main tasks is to design a filter that is capable of both approximation ability and fast response time.

Based on this new filter tailored for our specific task, we can develop

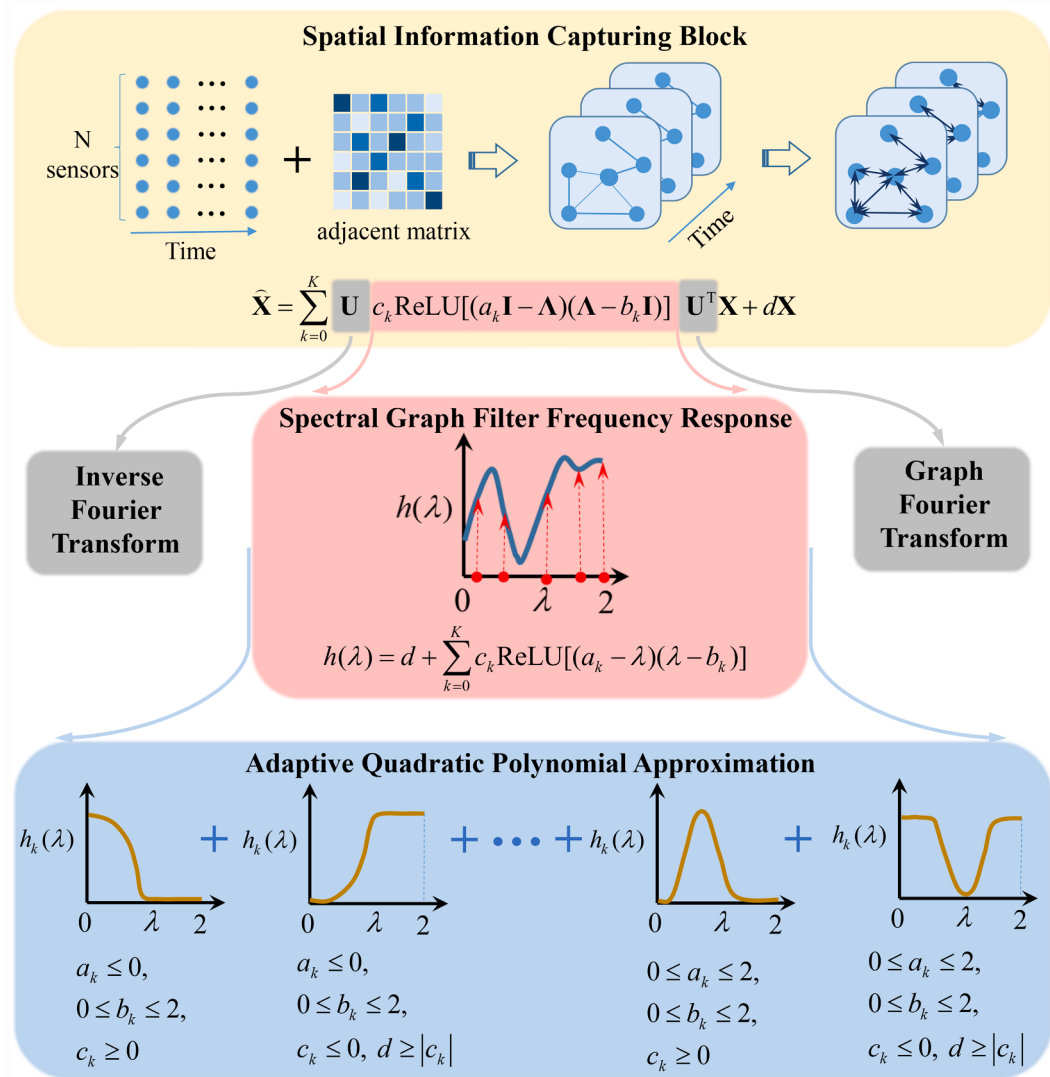


**Fig. 4.** An illustration of AQAGF. With different  $a_k$ ,  $b_k$ ,  $c_k$ , and  $d$ , not only Single-peak responses with positive or negative amplitude and arbitrary width can be achieved, but the low-pass, high-pass, band-pass, and band-stop filters can also be implemented. These typical filters can be combined to achieve any desired response function for a graph filter.

a spectral graph convolution neural network that can learn filter coefficients adaptively from training data. Unlike the methods mentioned in Section 2.3, our proposed method is interpretable. We can visualize its frequency response function and understand all of its behaviors in the frequency domain. We provide a detailed explanations and descriptions of our inspiration and spectral graph filtering approach in Section 4.2.

#### 4. Methodology

In this Section, we describe the method of constructing the graph structure in 4.1. In 4.2, we propose the Adaptive Quadratic Approximation Graph Filter (AQAGF), can transform into a fully interpretable spectral graph convolution neural network to capture spatial information. In 4.3, we present Interpretable Spatial-Temporal Graph Anomaly Detection (ISTGAD) based on ADAGF, which is an anomaly detection model with a transparent working mechanism. ISTGAD also demonstrates robustness to missing and noisy data, making it suitable for real-world satellite power system telemetry data.

##### 4.1. Graph structure construction

The inter-coupling relationship among the sensors of the power system remains unchanged over time, distinguishing it from other fields. Therefore, this work uses the static graph. Currently, the main methods for constructing graph structure within the GNN field include: similarity calculation, learning from data, and physical prior guidance. The first method is the most classic and widely used. The second has been increasingly employed in recent years but consumes computational resources. And the third has promising research prospects, however, it is not applicable to this study, as declared in Section 3.1, we believe that the third method, while beneficial for capturing physical correlations, might overlook some logical and data correlations. So we choose similarity calculation. Our graph structure is constructed as follows. First, a segment of training data is intercepted, denoted as  $\{\mathbf{l}_1, \dots, \mathbf{l}_N\}$ , where  $\mathbf{l}_i \in \mathbb{R}^{len}$  represents the observation from the  $i$ -th sensor  $o_i$ , and  $len$  is the length of intercepted observation. Then, the similarities among the sensors are calculated and the similarity between  $o_i$  and  $o_j$  is defined as:  $\text{sim}_{ij} = d(\mathbf{l}_i, \mathbf{l}_j)$ , where  $d(\cdot)$  is a similarity function, with options such as cosine similarity or Euclidean distance. Finally, for node  $o_i$ , the top  $M$  sensor nodes that are most similar to it to establish the edge connection

are selected, as shown in Eq. (6):

$$([o_i, o_j] \in E) \Leftrightarrow (\mathbf{A}_{ij} = 1), \text{ if } j \in \text{TopM}(\{\mathbf{sim}_{im} : m \in \{1, 2, \dots, N\} \setminus \{i\}\}), \quad (6)$$

where  $\text{TopM}(\cdot)$  denotes the indices of the highest  $M$  values among its inputs. The  $M$  can be chosen by the desired sparsity level, which refers to the number of edges connected to each node.

#### 4.2. Adaptive Quadratic Approximation Graph Filter (AQAGF)

First of all, we necessitate a polynomial expression that can approximate the desired arbitrary FRF shape with a low order and must be simple so that does not consume too much computational time. Our solution is to propose a novel graph filter based on the quadratic function: Quadratic Approximation Graph Filter (QAGF). Specifically, (1) Strategy of QAGF: the quadratic function is transformed into a function base that resemble the shape of a Gaussian distribution using ReLU (Rectified Linear Unit), quadratic function allows for flexible adjustment of scale and amplitude. Subsequently, multiple ReLU-transformed quadratic function bases are combined to approximate the desired FRF, akin to the strategy of GMM (Gaussian Mixture Model). (2) Advantages of QAGF: The FRFs of typical filters such as high-pass, low-pass, band-pass, and band-stop filters, as well as filters learned from real-world datasets (He et al., 2021), exhibit a pattern that is combined by bell-shaped, J-shaped and U-shaped curves. Therefore, based on the quadratic functions is advantageous as QAGF only requires simple calculations and low-order blending to achieve approximation. (3) Usefulness of QAGF: to demonstrate the usefulness of the QAGF in approximating arbitrary FRF, envisage the limiting case where multiple minimal-scaled quadratic functions are combined. Each function corresponds to a frequency component and captures its corresponding amplitude, resulting in a perfect approximation of the desired arbitrary FRF.

As shown in Fig. 4, the frequency response function of our proposed filter is:

$$h(\lambda) = d + \sum_{k=0}^K c_k \text{ReLU}[(a_k - \lambda)(\lambda - b_k)], \quad (7)$$

where  $a_k$  and  $b_k$  are two zero-points of the quadratic function,  $c_k$  is amplitude,  $d$  is the residual coefficient, and ReLU (Rectified Linear Unit) is a kind of non-linear activation function. The ReLU is crucial for the QAGF, without it the FRF would still be a quadratic function with a single peak no matter how many quadratic functions are added together. Therefore, ReLU is required to transform each quadratic function into a shape similar to a Gaussian kernel function. The residual coefficient  $d$  is also necessary, and if it is larger than a negative  $c_k$ , the combination of them can achieve a band-stop or high-pass filter. See Fig. 4 for details. Moreover, by adaptive learning of filter coefficients from training data, QAGF can be transformed into a spectral graph convolution neural network called AQAGF, which is defined as follows.

$$\widehat{\mathbf{X}} = \sum_{k=0}^K \mathbf{U} c_k \text{ReLU}[(a_k \mathbf{I} - \Lambda)(\Lambda - b_k \mathbf{I})] \mathbf{U}^\top \mathbf{X} + d \mathbf{X}, \quad (8)$$

where  $a_k$ ,  $b_k$ ,  $c_k$ , and  $d$  are trainable parameters. As claimed in 4.2, this work uses the static graph, which also helps conserve computational time. Despite AQAGF is a spectral convolution approach, the eigenvalue decomposition is computed only once and then  $\mathbf{U}$  and  $\Lambda$  are unchanged throughout training and testing phases.

Overall, as shown in Fig. 4, the architecture and implementation principle of AQAGF is as follows:

- Step One: Through ReLU and learning different parameters  $a_k$ ,  $b_k$ ,  $c_k$ ,  $d$ , respective forms of sub-filters are generated, such as single peak,

low-pass, high-pass, band-pass, and band-stop. They respectively extract or suppress corresponding frequency components.

- Step Two: These sub-filters are combined to achieve the required spectral graph filter frequency response function.
- Step Three: This FRF will be used to perform the graph filtering operation, which is also a process of extracting information from the data in the spatial dimension.

The key advantage of AQAGF lies in its ability to maintain the same level of computational resource consumption as commonly used GNNs, while also providing interpretability. In each quadratic term of Eq. (8),  $\mathbf{I}$  is an identity matrix,  $\Lambda$  is a diagonal matrix, and the entire term is just a simple quadratic operation. The computational resources required for a K-order AQAGF are similar to those required for a K-layer GCN, GAT, or GraphSAGE. However, AQAGF is not a black box model, AQAGF exhibits transparency by displaying its extracted and suppressed frequency components through frequency response functions. This capability facilitates further extraction of anomalous features that can be used in subsequent analysis for anomaly tracing, such as cause analysis and anomaly location.

#### 4.3. Interpretable Spatial-Temporal Graph Anomaly Detection (ISTGAD)

Based on AQAGF, we construct a practical anomaly detection model, ISTGAD, according to the data characteristics of satellite power telemetry data. Specifically, in addition to AQAGF, our proposed model, ISTGAD, mainly consists of the following techniques:

##### (1) Spatial-Temporal Graph

GNNs have drawn wide attention because of their excellent ability to capture spatial correlations. The spatial-temporal graph networks are one of its branches, which is most widely used in the traffic field to capture temporal and spatial correlations, simultaneously. Relevant works encompass STGCN (Yu et al., 2018), AGCRN (Bai et al., 2020), and other notable contributions in the field. The central idea is that spatial and temporal correlations are separately captured via a spatial information aggregation block and a temporal feature extraction block.

##### (2) Adversarial Training Strategy

In the preprocessing, we initially addressed missing values by piecewise constant interpolation. However, its capacity is restricted. Therefore, we introduce the adversarial strategy, which can make our model robust to missing data (Yoon et al., 2018) and generate reconstruction samples that are indistinguishable from real samples.

##### (3) Autoencoder Architecture

ISTGAD uses an autoencoder architecture because of its robustness to noise (Shang et al., 2023). A commonly accepted notion is that during the process of mapping data to high-dimensional representation and then reconstructing it back into the original space, only essential information is retained while noise is eliminated. The autoencoder architecture also enhances traceability by leveraging intermediate features, such as the reconstructed data and the high-dimensional space representation, which can potentially contribute to subsequent analyses (Wang et al., 2022).

The specific architecture of ISTGAD is shown in Fig. 5. The architecture details are as follows:

- The encoder consists of a spatial information aggregation block and a temporal feature extraction block to capture spatial and temporal correlations. The spatial information aggregation block is an AQAGF, its frequency response function can visually interpret which frequency bands are extracted by the encoder to reconstruct the sample

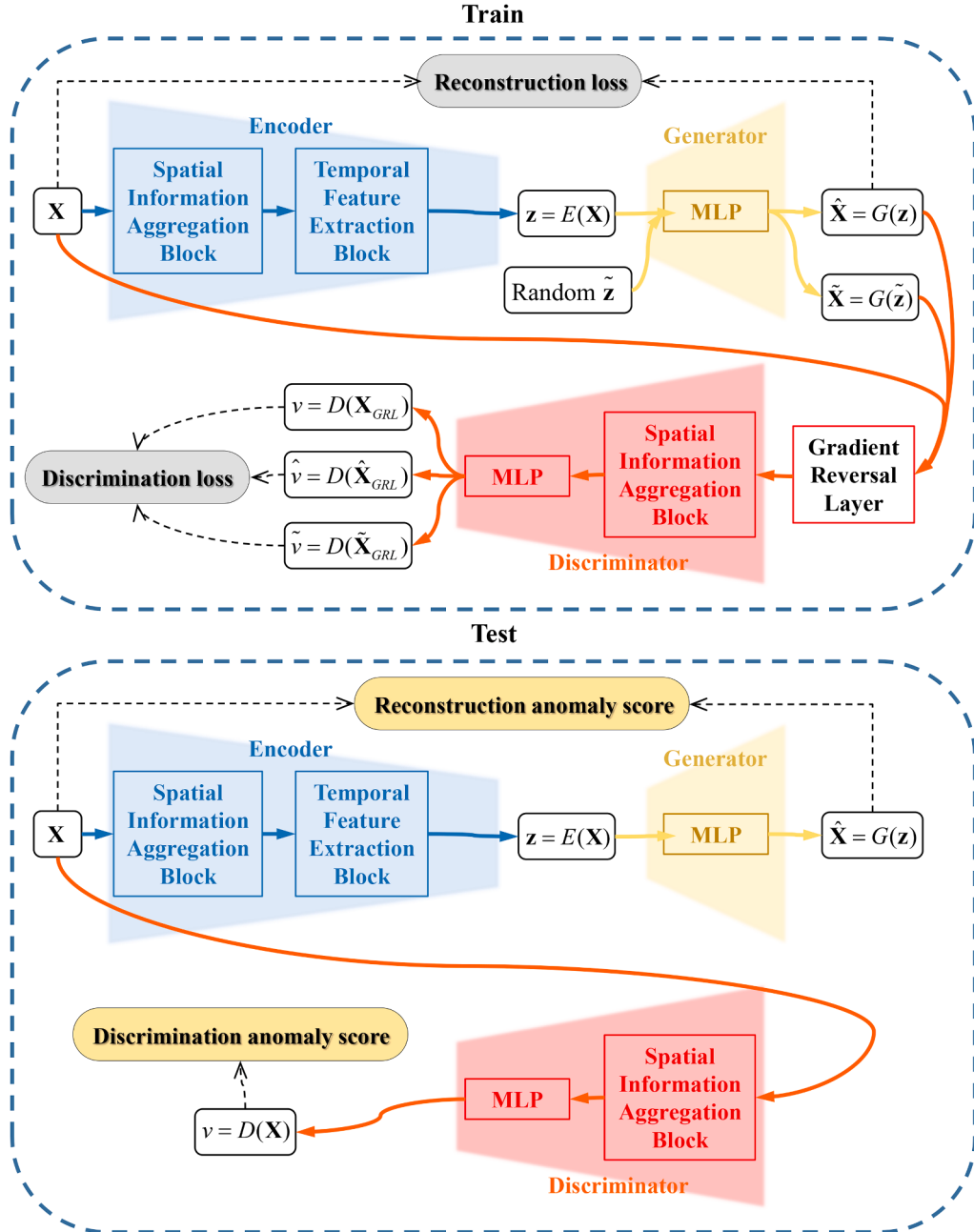


**Fig. 5.** An illustration of ISTGAD. The  $E()$ ,  $G()$ , and  $D()$  denote the encoder, generator, and discriminator respectively. The spatial information aggregation blocks are AQAGFs, and the temporal feature extraction block is dilated convolution or GRU.

- data. For the temporal feature extraction block, we use the dilated convolution or GRU.
- The generator is a multilayer perceptron (MLP).
  - The discriminator consists of an AQAGF and an MLP. The AQAGF is used to extract the discriminative information, and its frequency response function can visually interpret which frequency bands the ISTGAD focuses on to discriminate. The MLP maps the extracted features to a score value.
  - Additionally, to accelerate training, instead of employing iterative optimization, we introduce a Gradient Reversal Layer (GRL) into the ISTGAD. GRL is able to optimize the reconstruction part and the discrimination part in the opposite direction in a single gradient backpropagation step, achieving simultaneous optimization of the encoder, generator, and discriminator.

As shown in Fig. 5,  $E()$ ,  $G()$ , and  $D()$  denote the encoder, generator, and discriminator, respectively. During the training period, there are three information flows:

- Reconstruction information flow: The Encoder compresses the original data samples  $X$  into low-dimensional features and then the Generator reconstructs them as  $\hat{X}$ .
- Generation information flow: To guide the training of the discriminator and to enhance its generalization, we set random high-dimensional space representation  $\tilde{z}$ . The Generator creates random generated samples  $\tilde{X}$  from these random representations  $\tilde{z}$ .
- Discrimination information flow: The original samples  $X$ , reconstructed samples  $\hat{X}$ , and random generated samples  $\tilde{X}$  are discriminated by the Discriminator, and obtain the discrimination scores  $v$ ,  $\hat{v}$ , and  $\tilde{v}$ , respectively.

And the training loss is defined as:

$$\begin{aligned} L &= \alpha \cdot L_R + L_D, \\ L_R &= \text{MAE}(\mathbf{X} - \hat{\mathbf{X}}) = \text{MAE}(\mathbf{X} - G(E(\mathbf{X}))), \\ L_D &= -|\nu - \tilde{\nu}| + \epsilon \cdot \max(\nu - \tilde{\nu}, 0) - |\nu - \tilde{\nu}| + \epsilon \cdot \max(\nu - \tilde{\nu}, 0), \end{aligned} \quad (9)$$

where  $L$  is the training loss, which consists of the reconstruction loss  $L_R$  and the discrimination loss  $L_D$ , and  $\alpha$  is the trade-off coefficient. The reconstruction loss is the Mean Absolute Error (MAE) of the input sample  $\mathbf{X}$  and the reconstructed sample  $\hat{\mathbf{X}}$ , which is used to equip ISTGAD with data reconstruction capabilities. The first term of the discriminative loss is to make a difference between the discriminative scores of normal samples and non-normal samples, the second term is to ensure that the discriminator gives greater discriminative scores to non-normal samples rather than normal samples, and the  $\epsilon$  is the trade-off parameter, the third and fourth terms are set for the same reason.

During the test period, there is no longer the random high-dimensional space representation  $\tilde{\mathbf{z}}$  and no need to discriminate the reconstructed data, the anomaly score for (sensor  $i$ , and timestamp  $t$ ) is defined as:

$$S_{i,t} = |\mathbf{x}_{i,t} - \hat{\mathbf{x}}_{i,t}| + \delta \cdot \nu = |\mathbf{x}_{i,t} - \hat{\mathbf{x}}_{i,t}| + \delta \cdot D(\mathbf{X}), \quad (10)$$

where  $D$  means the discriminator, and  $\delta$  is the trade-off parameter. The anomaly score consists of the reconstruction error and the discrimination score. We provide anomaly scores for each sensor at each timestamp, which may support subsequent analysis. Inspired by (Deng and Hooi, 2021), we will use robust normalization and simple moving average (SMA) for the two score terms to balance different scales and obtain smoothed scores. In the end, we adopt the maximum value of each sensor's anomaly score as the final anomaly score at that timestamp:  $s_t = \max_i S_{i,t}$ , which will be used to output the anomaly timestamps ( $s_t$  exceeds a fixed threshold), and the specific threshold setting is also the same as (Deng and Hooi, 2021).

## 5. Experiments

Our experiments are divided into Experiment I and Experiment II. Experiment I aims to validate the anomaly detection performance of ISTGAD, Experiment II aims to verify the landing practicality and visual working mechanism interpretation. Experiment I used the datasets Mars Science Laboratory (MSL) and Soil Moisture Active and Passive (SMAP) (Hundman et al., 2018), which are widely acknowledged as effective evaluation datasets in the field of multidimensional time series anomaly detection. These datasets have been widely used in various anomaly detection methods. We will compare our method with other baseline methods using these two datasets to showcase its performance in anomaly detection. Experiment II used the dataset BIRDS (Cespedes et al., 2022), a new dataset publicly released by Cespedes et al. in 2022. Although its usage is not yet widespread, this dataset comprises real-world observational data that accurately reflects the demand for anomaly detection in satellite power systems. We apply our method to this dataset for the purpose of validating its practicality, while also visualizing the working mechanism of our method to demonstrate its interpretability.

### 5.1. Dataset

Both Mars Science Laboratory (MSL) and Soil Moisture Active Passive (SMAP) are widely used spacecraft telemetry data for anomaly detection. MSL is the observation data from the Mars Science Laboratory rover: Curiosity, launched by NASA. SMAP is the observation data of the US Earth observation satellite used to observe soil moisture. They are expert-labeled by spacecraft engineers, with the training data devoid of anomalies while the test data includes anomalies. Please refer to Table 1 for further details. These two datasets are widely used in the field of time

**Table 1**  
MSL and SMAP details.

Dataset	MSL	SMAP
Feature Description	temperature, radiation, power, etc.	radar data, soil moisture, radiation, etc.
telemetry channels	55	27
Training size	58,317	135,183
Testing size	73,729	427,617
Anomaly rate (%)	10.29	13.13

series anomaly detection and are recognized as effective baseline datasets. As real-world telemetry datasets from spacecraft, they possess typical data characteristics of telemetry signal in space environment, the anomalies within these datasets are complex and diverse. They can fully reflect the demands of practical engineering applications.

BIRDS consists of samples from Tsuru (25653 timestamp), Nepalisat (3040 timestamp), Raavana (2159 timestamp), and Uguisu (3270 timestamp) Satellites. These satellites are all 1U CubeSat units based on the same open-source standardized bus designed by Kyutech, and share identical EPS (Electrical Power System) design. Details can be found in (Cespedes et al., 2022). We completed the labeling and dataset partitioning based on the anomaly criteria described in (Cespedes et al., 2022). Due to the significant imbalance in the lengths of the four subdatasets and the presence of anomalies only in Raavana and Uguisu, the last two subdatasets almost all the sliding window samples are anomalies, while the first two subdatasets are all normal samples. So our training data is solely derived from the Tsuru satellite, which may lead to inconsistent data distribution. This inconsistent data distribution is inevitable and is a challenge that intelligent methods must confront when applied to practical tasks. Because when performing health management for an already launched or yet-to-be-launched satellite, we always have only a small amount of or no operational data from that satellite. It is inevitable that we encounter issues such as insufficient actual measurement data, unsupervised learning, inconsistent sampling frequencies, data missing, and highly noise. But we solved this inconsistent data distribution problem by capturing spatial and temporal information simultaneously, although temporal information is strongly affected by this problem, but spatial information has inherent resilience, the coupling relationships between sensors are universal across the four satellites, exhibiting the same patterns on all four satellites. We learn spatial correlations from the Tsuru satellite and apply them to other satellites. The details and results will be shown in subsequent sections. Specifically, we concatenated the four subdatasets in the order Tsuru, Nepalisat, Raavana, and Uguisu, and then set the first 65 % as the training set and the last 35 % as the test set, shown in Fig. 6.

### 5.2. Pre-processing

#### (1) Piecewise Constant Interpolation

We use piecewise constant interpolation to fill the missing values, which actually just replaces each missing value with its preceding value. It is simple, effective and not easily misled by noise to generate other anomalous values (Yairi et al., 2017).

#### (2) Windowed Averaging

We employ window averaging to primitively deal with the noise in the data. The principle is to replace the values in the window with their average value, see (Cespedes et al., 2022) for details. And we also use the suggested values in (Cespedes et al., 2022) as the window size.

#### (3) Min-Max Normalization

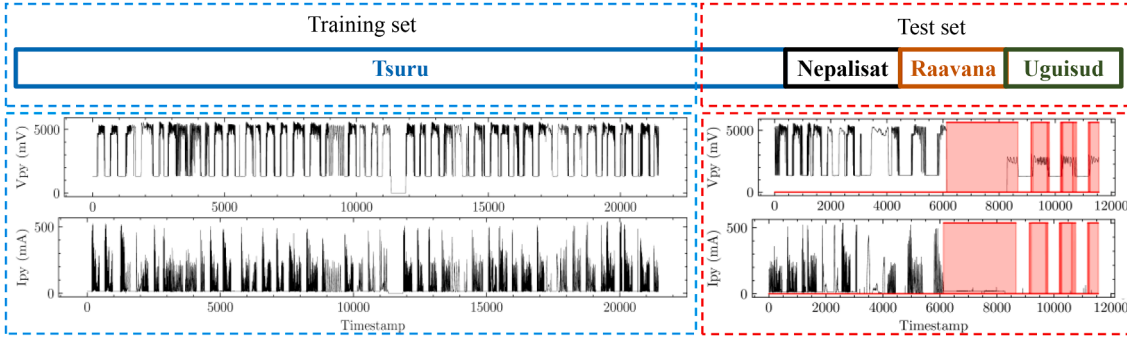


**Fig. 6.** An illustration of the BIRDS dataset. The red areas indicate the occurrence of anomalies. (For interpretation of the references to color in this figure legend, the reader is referred to the web version of this article.)

Minimum-maximum normalization, also known as discrete standardization, is a linear transformation of original data. It can preserve the relationships among original data values and map them to [0,1], which is conducive to the training and convergence of neural networks.

### 5.3. Experimental details

Some experimental details are as follows:

- The temporal feature extraction block employs GRU, with the number of layers set to 1, and the channel of the hidden layer equal to the graph node number.
- The similarity function  $d(\cdot)$  employs Euclidean distance for BIRDS and cosine similarity for MSL and SMAP.
- The encoding-decoding framework of AQAGF opts for the standard autoencoder over the variational autoencoder, implying that there are no constraints imposed on the distribution of the high-dimensional space representation. Because it focus more on data compression, feature learning, and anomaly detection.
- The data publishers of the BIRDS dataset have identified real-world anomalies in the dataset, specifically, the Raavana satellite experienced a Solar Panel Anomaly, and the Uguisud satellite suffered from a Solar Cell Anomaly. These information were used to label the dataset.
- The discriminator spatial information aggregation block can either directly feed the filtered time domain data into the MLP, or multiply it with  $U^\top$  to transform it into frequency domain data and then feed it into the MLP, each of them has its own applicable case, in our experiments, MSL and BIRDS utilize the former method, while SMAP employs the latter.

### 5.4. Experiment I

#### 5.4.1. Baselines

We compared our method with the widely used baselines in the same field: Deep-SVDD (Ruff, 2018), LSTM-VAE (Park et al., 2018), LSTM-NDT (Hundman et al., 2018), DAGMM (Zong et al., 2018), OmniAnomaly (Su et al., 2019), and the nearly three years advanced method: MERLIN (Nakamura et al., 2020), ITAD (Shin, et al., 2020), MTAD-GAT (Zhao, et al., 2020), USAD (Audibert et al., 2020), MAD-GAN (Li et al., 2019), and some typical machine learning anomaly detection methods: OCSVM (Tax and Duin, 2004), LOF (Breunig et al., 2000), Isolation Forest (Liu et al., 2008).

#### 5.4.2. Metrics

We employ the Precision, Recall, and F1-score, which are widely recognized evaluation metrics in the field of anomaly detection, to evaluate the performance of each method. Precision is the ratio of correctly predicted positive observations to the total predicted positive

observations, reflects the percentage of detected anomalies are true anomalies. Recall is the ratio of correctly predicted positive observations to all observations in the actual class, reflects the proportion of correctly identified anomalies among all true anomalies. F1-Score is a weighted average of Precision and Recall, identifies the overall performance of the anomaly detection model by combining both Recall and Precision. They are calculated as:

$$\begin{aligned} \text{Precision} &= \frac{\text{True Positive}}{(\text{True Positive} + \text{False Positive})}, \\ \text{Recall} &= \frac{\text{True Positive}}{(\text{True Positive} + \text{False Negative})}, \\ \text{F1-Score} &= \frac{2 * (\text{Recall} * \text{Precision})}{(\text{Recall} + \text{Precision})}. \end{aligned} \quad (11)$$

#### 5.4.3. Result

The results of Experiment I are shown in Table 2. The level of detection performance is represented by a color gradient ranging from blue to red, with blue indicating poor performance and red indicating excellent performance. Specifically, we set up a data-missing experiment with 30 % of the input data artificially removed, and the results (penultimate row) proved that our model still maintained a quite good anomaly detection capability. The emphasis should be placed on the fact that some other methods in the table may show a high precision or recall, but this does not mean their methods are superior to ours. In fact, such an imbalance between precision and recall indicates a significant occurrence of either missed alarms or false alarms. The evaluation of method superiority should primarily consider the F1-score, as F1-score is the harmonic mean of Precision and Recall, which represents the comprehensive anomaly detection performance. Clearly, our method (the last two rows) exhibits the best overall anomaly detection performance, as evidenced by its occupation of the largest red area. Our method not only outperforms other methods in terms of F1-score metrics, but also maintains advanced level anomaly detection performance even when 30 % of the data was missing. This indicates that the implementation of adversarial training strategy enables the model to acquire comprehensive proficiency in handling missing data, thereby augmenting its capacity to deceptively recover data, ultimately improving its robustness and generalization capabilities. In conclusion, our model has achieved satisfactory experimental results, thanks to the following points: First, our model was developed with a focus on the data characteristics of real-world space telemetry scenarios, exhibiting robustness to noise and data missing. Secondly, our approach effectively captures both spatial and temporal information, enabling a more comprehensive data mining. Given these strengths, it is foreseeable that our method will perform well on typical space telemetry datasets such as MSL and SMAP, where there is a strong logical correlation between channels.

**Table 2**

Anomaly detection results of Experiment I. The P, R, and F1 represent the Precision, Recall, and F1-score (as %) respectively. The term 'Ours (0.3)' indicates that 30% of the input data is artificially missing.

Dataset	MSL			SMAP			
	Metric	P	R	F1	P	R	F1
MERLIN		26.13	46.45	33.45	15.77	99.99	27.25
LOF		47.72	85.25	61.18	58.93	56.33	57.60
Isolation Forest		53.94	86.54	66.45	52.39	59.07	55.53
OCSVM		59.78	86.87	70.82	53.85	59.07	56.34
Deep-SVDD		91.92	76.63	83.58	89.93	56.02	69.04
ITAD		69.44	84.09	76.07	82.42	66.89	73.85
LSTM-VAE		85.49	79.94	82.62	92.20	67.75	78.10
LSTM-NDT		62.88	100.00	77.21	85.23	73.26	78.79
DAGMM		73.63	100.00	84.82	86.45	56.73	68.51
OmniAnomaly		78.48	99.24	87.65	81.30	94.19	87.28
MTAD-GAT		79.17	98.24	87.68	79.91	99.91	88.80
USAD		79.49	99.12	88.22	74.80	96.27	84.19
MAD-GAN		85.16	99.30	91.69	81.57	92.16	86.54
Ours (0.3)		84.66	99.93	91.67	86.67	92.28	89.38
Ours		85.22	99.42	91.77	81.20	100.00	89.62

### 5.5. Experiment II

Applying our method to the BIRDS dataset, we obtained precision = 0.8703, recall = 0.9835, and F1-score = 0.9235, which demonstrates that ISTGAD has practical value. We visualized the anomaly detection

results of two representative channels (an abnormal voltage channel and a normal voltage channel) in Fig. 7.

As stated in Section 5.1, the real-world data exhibit inconsistent data distribution. By observing Fig. 6, it can be noticed that in the training set, the trend of the data remains stable throughout, with the

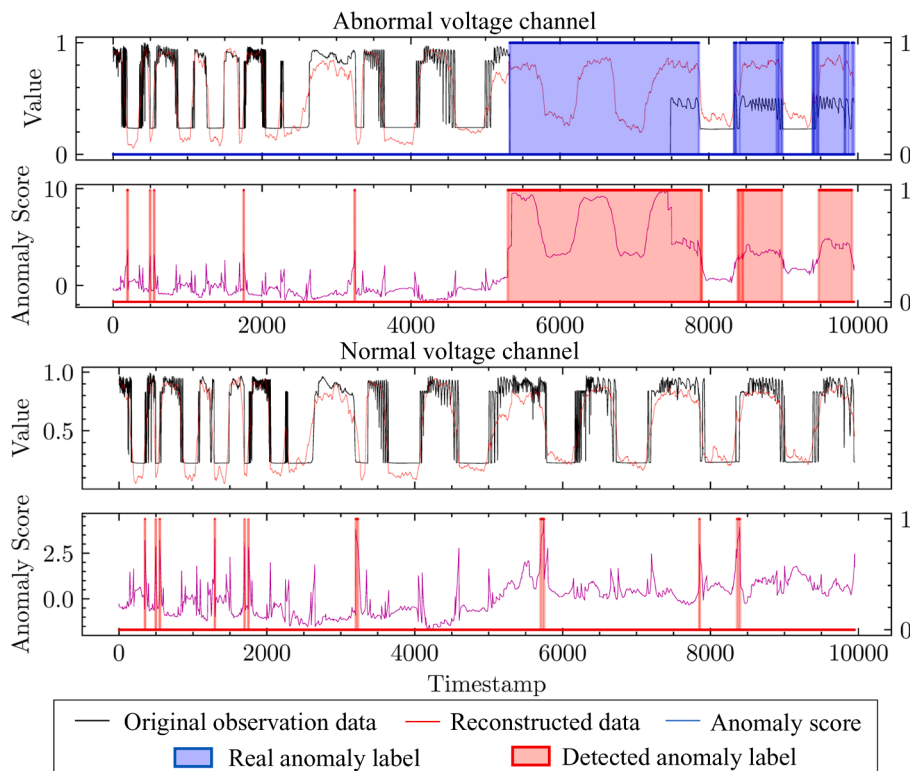


**Fig. 7.** Anomaly detection results visualization. The upper two frames are abnormal voltage and current channels, while the lower two frames are normal voltage and current channels.

charge-discharge cycle consistently maintained at around 500 timestamps. However, in the test set, the data cycles are different from the training set and constantly changing. Within the range of 0 ~ 2000 timestamps (belonging to Tsuru satellite), the cycle maintained at around 500 timestamps. Within the range of 2000 ~ 5000 timestamps (belonging to NepalSat satellite), the cycle becomes uncertain and chaotic. Within the range of 5000 ~ 10000 timestamps (belonging to Raavana and Uguisud satellites), the cycle maintained at around 1000 timestamps. Due to the inconsistent and chaotic temporal information, it is not possible to perform this reconstruction task using methods that only focus on temporal correlations. However, as shown in Fig. 7, our method has effective data reconstruction (the red line) and excellent anomaly detection capability. The cycles of the data fragments we reconstructed precisely align with the aforementioned description. This was accomplished by aggregating information sourced from other sensors, such as the current and temperature channels of the same solar panel and the voltage channel of other solar panels. This phenomenon supports our opinion that the graph structure can capture spatial correlations, and highlights the indispensability of attending to and exploiting spatial correlation in various multidimensional time series data mining tasks. In addition, the autoencoder architecture also demonstrates its efficacy. The reconstructed data exhibit a higher degree of smoothness compared to the original data, the autoencoder effectively eliminates the pronounced noise disturbance that present in the original data and exhibits a robust adaptive capability. In summary, benefiting from the spatial correlation capturing capability of AQAGF, the issue of inconsistent data distribution in BIRDS is resolved, achieving excellent

results in data reconstruction and anomaly detection. We believe that our method can guarantee good performance on strongly coupled sensors datasets, and within a certain range, the more sensors there are and the more significant the correlations, the better the data mining outcomes will be.

To investigate the working mechanism of ISTGAD, we analyzed the data flow of ISTGAD depicted in Fig. 5 and extracted several pivotal points: the filtering of the Encoder AQAGF, the high-dimensional space representation  $\mathbf{z}$  obtained by the Encoder, the reconstructed  $\hat{\mathbf{X}}$  obtained from the Generator, the filtering of the Discriminator AQAGF, and the discriminative scores  $\mathbf{s}$  obtained from the Discriminator. Except for the reconstructed  $\hat{\mathbf{X}}$ , we will visualize and interpret each of them.

#### (a) Filtering of the AQAGFs

As we described in Section 4.2, the AQAGF filter is able to plot the frequency response function (FRF) as shown in Fig. 8. The FRF of the Encoder AQAGF can tell the researchers which frequency bands are associated with the reconstructed information, and the FRF of the Discriminator AQAGF can tell the researchers which frequency bands are associated with the discriminative information. The difference between them is where abnormal information gathers.

By analyzing Fig. 8, it is evident that, in contrast to the reconstruction information which primarily focuses on the middle frequency band surrounding 1.0, the discriminative information significantly amplifies the low-frequency band of 0 ~ 0.5 and the high-frequency band of 1.5 ~

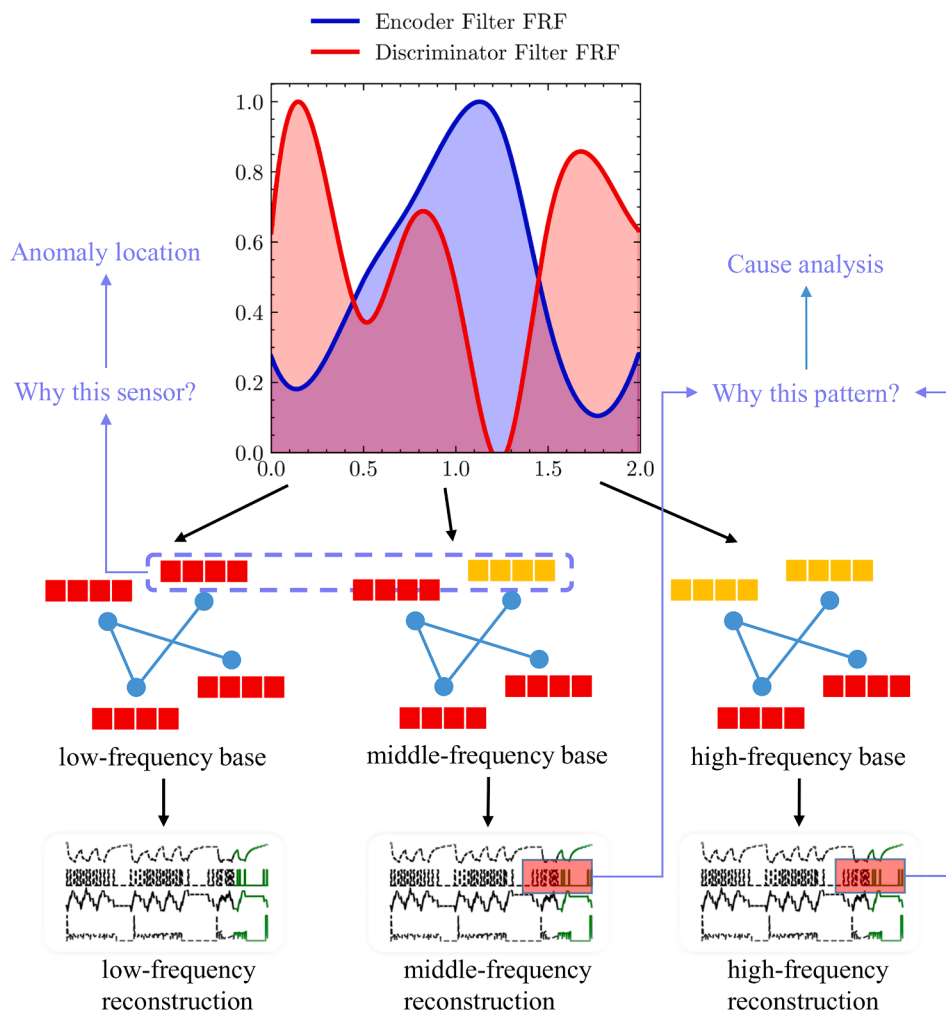


**Fig. 8.** The frequency response function of the AQAGFs.

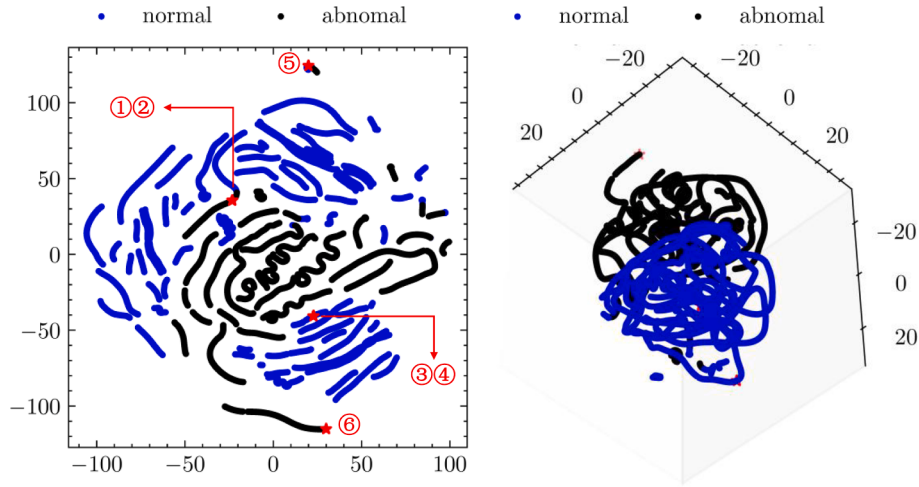


**Fig. 9.** T-SNE visualization of the high-dimensional space representation.

2. The abnormal information may be distributed in the frequency bands of  $0 \sim 0.5$  and  $1.5 \sim 2$ . After corresponding analysis, we can further extract some time-domain features from certain frequency bands. These time-domain features, along with the intermediate features of ISTGAD, such as the reconstructed data and the discriminator filtered data, can be directly used in subsequent analysis for anomaly tracing, such as cause analysis and anomaly location. In fact, a more in-depth study can be carried out in conjunction with (Tang et al., 2022), which is our next step. In terms of our current study, the phenomenon of spectrum right-shifting caused by the anomaly (Tang et al., 2022) is not prominently observed in multidimensional time-series data such as BIRDS. This paper focuses on the anomaly detection method and its interpretability, so we will not discuss this more for now. Moreover, it can also be seen that the AQAGF does not suffer from over-smoothing, it achieves a FRF of any

desired shape, rather than just low-pass filtering.

#### (b) The high-dimensional space representation

We plotted the two-dimensional and three-dimensional t-SNE (t-distributed stochastic neighbor embedding) diagrams of the high-dimensional space representation  $\mathbf{z}$  obtained from the Encoder, as shown in Fig. 9. The 3D t-SNE diagram shows that ISTGAD distinguishes well between normal and abnormal samples, which proves its excellent performance.

Further, in order to explain the meaning of  $\mathbf{z}$ , we calculate the two k-means clustering centers of the 2D t-SNE graph as ① and ③, the closest points to them as ② and ④, and the farthest points from them as ⑤ and ⑥. By drawing their corresponding sample data as shown in Fig. 10, we

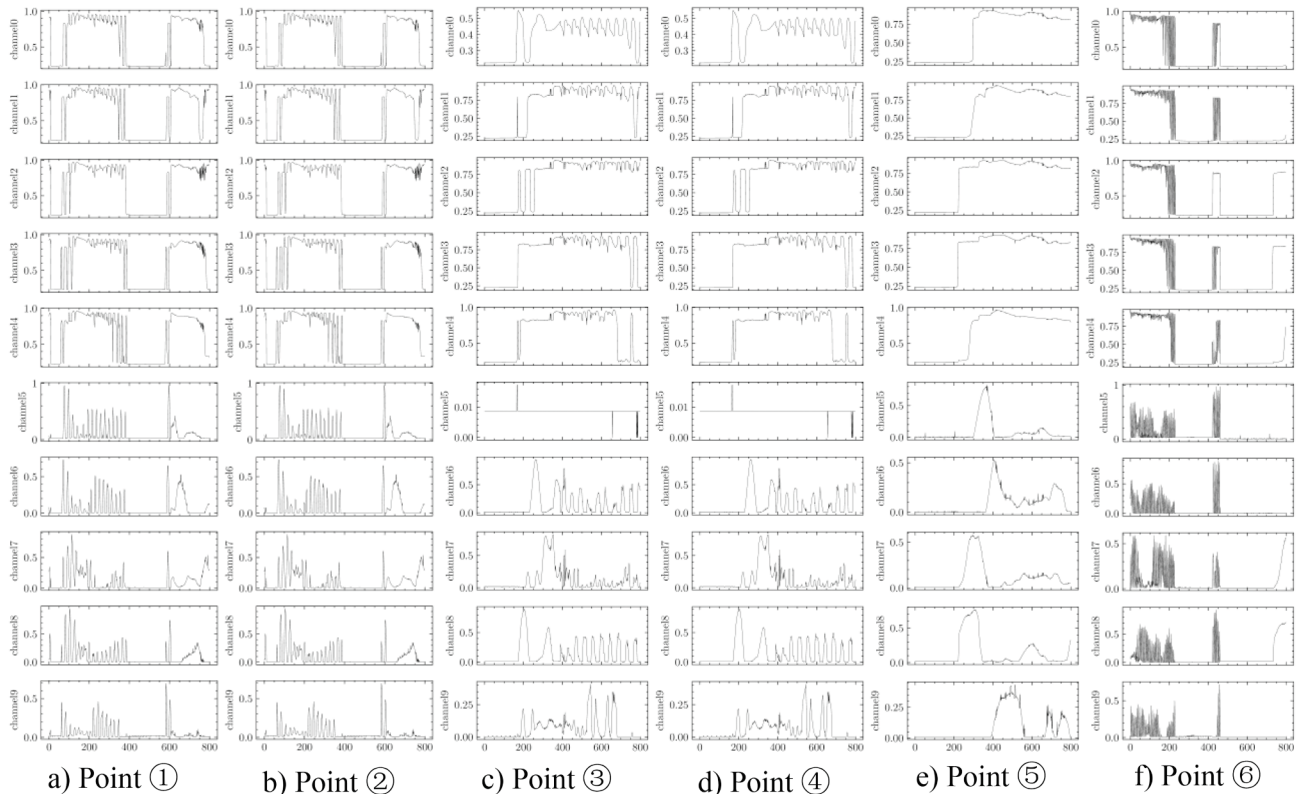


**Fig. 10.** The samples corresponding to the typical high-dimensional space representations.

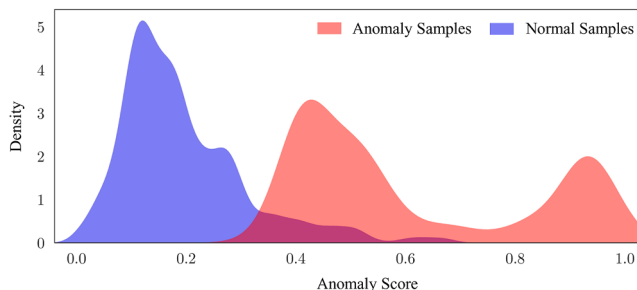


**Fig. 11.** An illustration of the discriminative scores distribution.

can find that the essence of the Encoder is the mapping of the sample features to the point coordinates in the high-dimensional space.

### (c) The discriminative scores $\mathbf{s}$ .

To visualize discriminative scores  $\mathbf{s}$ , we plotted the kernel density estimates of the discriminative scores, as shown in Fig. 11. It can be seen that abnormal samples are more widely distributed in the feature space and have significant differences from the distribution of normal samples. This difference in distribution signifies the effective identification capability of our model towards abnormal samples. Our model transforms the positional differences between abnormal samples and normal samples in the feature space into distributional differences of anomaly scores, and then distinguishes normal samples from abnormal samples based on these distributional differences.

## 6. Conclusions

This work proposes ISTGAD, a novel approach for anomaly detection in real-world telemetry data of satellite power systems. It is able to capture temporal and spatial correlations together, which is experimentally prove its necessity and superiority. As a transparent working mechanism method, ISTGAD possesses trustworthiness, traceability and guidance, which can effectively detect anomalies in an interpretable manner and provide valuable assistance for subsequent health management of O&M team. At the same time, ISTGAD also exhibits good robustness to noise and data missing, meaning that even when there are strong noise and missing values in the satellite power system telemetry data, ISTGAD is still able to produce excellent anomaly detection.

We believe that our method overcomes several potential challenges in real-world deployments. (a) Data source and quality: Although satellites transmit vast amounts of normal or abnormal data to ground stations, the quality of these data is poor, exhibiting high noise and data missing. However, our method demonstrates robustness against such issues. (b) Ease of understanding and optimization: The decisions made by the model need to be transparent, facilitating operators' understanding and trust in its decisions, as well as enabling further optimization and adjustments. Our method benefits from its interpretability, exhibiting trustworthiness, traceability, and guidance. (c) Computing resources: Factors such as computing resources are also ensured since our method is targeted for deployment at ground stations in a space-ground-integration operation.

In our future work, our attempts will include the following aspects: attempting to embed physical knowledge when establishing graph structures, endeavoring to apply the concept of DTW to GNNs, further delving into the frequency domain differences between normal and anomalous samples, exploring even rarer and more complex anomaly detection scenarios, extending our model to other multidimensional coupled data mining domains that require interpretability, and challenging other IoT data analysis tasks in harsh working conditions.

## Nomenclature

$G$	Graph
$o_i, o_j$	Node $i$ and Node $j$
$(o_i, o_j)$	Edge between nodes $o_i$ and $o_j$
$O, E$	Set of nodes and edges
$\mathbf{A}$	Adjacency matrix
$\mathbf{D}$	Degree matrix
$\mathbf{L}, \tilde{\mathbf{L}}$	Laplacian matrix and its symmetrically normalized format
$\mathbf{U}$	Eigenmatrix
$\Lambda$	Eigenvalue diagonal matrix
$\mathbf{I}$	Identity matrix
$\lambda$	Eigenvalue
$h(\cdot)$	Frequency Response Function
$K$	Order of the polynomial
$a_k, b_k, c_k$ , and $d$	Trainable parameters
$N$	Sensor/node number
$L$	Sample length
$i$	The $i$ -th sensor/node
$t$	The $t$ -th timestamp
$E(\cdot), G(\cdot)$ , and $D(\cdot)$	Encoder, Generator, and Discriminator
$\mathbf{X}$	Original input sample
$\hat{\mathbf{X}}$	Reconstructed sample
$\tilde{\mathbf{X}}$	Random reconstructed sample
$\mathbf{z}$	Encoder representation of $\mathbf{X}$
$\tilde{\mathbf{z}}$	Random encoder representation
$v, \hat{v}$ , and $\tilde{v}$	Discrimination scores of $\mathbf{X}$ , $\hat{\mathbf{X}}$ and $\tilde{\mathbf{X}}$
$L_R$	Reconstruction loss
$L_D$	Discrimination loss
$L$	Training loss
$\alpha, \epsilon$ and $\delta$	Trade-off parameters
$\mathbf{S}$	Anomaly score matrix

## Declaration of competing interest

The authors declare that they have no known competing financial interests or personal relationships that could have appeared to influence the work reported in this paper.

## Data availability

I have shared the link to my data/code at the Attach File step

## Acknowledgements

This work was supported by the Natural Science Foundation of China under Grand U22B2013, Fundamental Research Funds for the Central Universities (xzy022023060). We thank Dr. Zhi Zhai, Dr. Zhibin Zhao, and Dr. Fujin Wang for their constant guidance and support throughout the research. We also thank Dr. Xuefeng Chen for providing funding and project support.

## References

- J. Audibert, P. Michiardi, F. Guyard, S. Marti, and M. A. Zuluaga, “USAD: UnSupervised Anomaly Detection on Multivariate Time Series,” presented at the Proceedings of the 26th ACM SIGKDD International Conference on Knowledge Discovery & Data Mining, Virtual Event, CA, USA, 2020. [Online]. Available: <https://doi.org/10.1145/3394486.3403392>.
- Bai, M., et al. (2024). Deep graph gated recurrent unit network-based spatial-temporal multi-task learning for intelligent information fusion of multiple sites with application in short-term spatial-temporal probabilistic forecast of photovoltaic power. *Expert Systems With Applications*, 240, Article 122072. <https://doi.org/10.1016/j.eswa.2023.122072>
- Bai, L., Yao, L., Li, C., Wang, X., & Wang, C. (2020). Adaptive graph convolutional recurrent network for traffic forecasting. Presented at the Proceedings of the 34th International Conference on Neural Information Processing Systems, Vancouver, BC, Canada.
- S. Baireddy et al., “Spacecraft Time-Series Anomaly Detection Using Transfer Learning,” in 2021 IEEE/CVF Conference on Computer Vision and Pattern Recognition Workshops (CVPRW), 19-25 June 2021 2021, pp. 1951-1960, doi: 10.1109/CVPRW53098.2021.00223.
- Binxin, Y., Jinyuan, G., & Tao, H. (2013). Introduction to the latest high reliability space power standard in USA. *Aerospace Standardization*, 1, 38–41.

- Bosman, H. H. W. J., Iacca, G., Tejada, A., Wörtche, H. J., & Liotta, A. (2017). Spatial anomaly detection in sensor networks using neighborhood information. *Information Fusion*, 33, 41–56. <https://doi.org/10.1016/j.inffus.2016.04.007>
- Breunig, M. M., Kriegel, H.-P., Ng, R. T., & Sander, J. (2000). LOF: Identifying density-based local outliers. *SIGMOD Rec.*, 29(2), 93–104. <https://doi.org/10.1145/335191.3355388>
- Carlton, A., Morgan, R., Lohmeyer, W., & Cahoy, K. (2018). Telemetry fault-detection algorithms: applications for spacecraft monitoring and space environment sensing. *Journal of Aerospace Information Systems*, 15(5), 239–252. <https://doi.org/10.2514/1.I010587>
- A. J. J. Cespedes, B. H. B. Pangestu, A. Hanazawa, and M. Cho, "Performance Evaluation of Machine Learning Methods for Anomaly Detection in CubeSat Solar Panels," *Applied Sciences*, vol. 12, no. 17, p. 8634, 2022. [Online]. Available: <https://www.mdpi.com/2076-3417/12/17/8634>.
- Chen, Z., Chen, D., Zhang, X., Yuan, Z., & Cheng, X. (2022). Learning Graph Structures With Transformer for Multivariate Time-Series Anomaly Detection in IoT. *IEEE Internet of Things Journal*, 9(12), 9179–9189. <https://doi.org/10.1109/JIOT.2021.3100509>
- W. Chen, L. Tian, B. Chen, L. Dai, Z. Duan, and M. Zhou, "Deep Variational Graph Convolutional Recurrent Network for Multivariate Time Series Anomaly Detection," presented at the Proceedings of the 39th International Conference on Machine Learning, Proceedings of Machine Learning Research, 2022. [Online]. Available: <https://proceedings.mlr.press/v162/chen22x.html>.
- Chien, E., Peng, J., Li, P., & Milenkovic, O. (2021). Adaptive Universal Generalized PageRank Graph Neural Network. *International Conference on Learning Representations*.
- Dai, E., & Chen, J. (2022). Graph-augmented normalizing flows for anomaly detection of multiple time series. *International Conference on Learning Representations*.
- Defferrard, M., Bresson, X., & Vandergheynst, P. (2016). Convolutional neural networks on graphs with fast localized spectral filtering. *Advances in Neural Information Processing Systems*, 29.
- A. Deng and B. Hooi, "Graph Neural Network-Based Anomaly Detection in Multivariate Time Series," *Proceedings of the AAAI Conference on Artificial Intelligence*, vol. 35, no. 5, pp. 4027–4035, 05/18 2021, doi: 10.1609/aaa.v35i1.16523.
- S. Dheepadharshani, S. Anandh, K. B. Bhavinaya, and R. Lavanya, "Multivariate Time-series Classification for Automated Fault Detection in Satellite Power Systems," in *2019 International Conference on Communication and Signal Processing (ICCP)*, 4-6 April 2019 2019, pp. 0814–0817, doi: 10.1109/ICCP.2019.8698017.
- Ding, C., Sun, S., & Zhao, J. (2023). MST-GAT: A multimodal spatial-temporal graph attention network for time series anomaly detection. *Information Fusion*, 89, 527–536. <https://doi.org/10.1016/j.inffus.2022.08.011>
- Grattarola, D., Zambon, D., Livi, L., & Alippi, C. (2020). Change detection in graph streams by learning graph embeddings on constant-curvature manifolds. *IEEE Transactions on Neural Networks and Learning Systems*, 31(6), 1856–1869. <https://doi.org/10.1109/TNNLS.2019.2927301>
- Hamilton, W., Ying, Z., & Leskovec, J. (2017). Inductive representation learning on large graphs. *Advances in neural information processing systems*, 30.
- He, M., Wei, Z., & Wen, J.-R. (2022). Convolutional Neural Networks on Graphs with Chebyshev Approximation, Revisited. *Advances in Neural Information Processing Systems*.
- He, M., Wei, Z., & Xu, H. (2021). Bernnet: Learning arbitrary graph spectral filters via bernstein approximation. *Advances in Neural Information Processing Systems*, 34, 14239–14251.
- He, Z., Xu, L., Yu, J., & Wu, X. (2024). Dynamic multi-fusion spatio-temporal graph neural network for multivariate time series forecasting. *Expert Systems with Applications*, 241, Article 122729. <https://doi.org/10.1016/j.eswa.2023.122729>
- K. Hundman, V. Constantinou, C. Laporte, I. Colwell, and T. Soderstrom, "Detecting Spacecraft Anomalies Using LSTMs and Nonparametric Dynamic Thresholding," presented at the Proceedings of the 24th ACM SIGKDD International Conference on Knowledge Discovery & Data Mining, London, United Kingdom, 2018. [Online]. Available: <https://doi.org/10.1145/3219819.3219845>.
- H. Jiang, K. Zhang, J. Wang, X. Wang, and P. Huang, "Anomaly Detection and Identification in Satellite Telemetry Data Based on Pseudo-Period," *Applied Sciences*, vol. 10, no. 1, p. 103, 2020. [Online]. Available: <https://www.mdpi.com/2076-3417/10/1/103>.
- W. Jin, S. Zhang, B. Sun, P. Jin, and Z. Li, "An Analytical Investigation of Anomaly Detection Methods Based on Sequence to Sequence Model in Satellite Power Subsystem," *Sensors*, vol. 22, no. 5, doi: 10.3390/s22051819.
- W. Jin, B. Sun, Z. Li, S. Zhang, and Z. Chen, "Detecting Anomalies of Satellite Power Subsystem via Stage-Training Denoising Autoencoders," *Sensors*, vol. 19, no. 14, doi: 10.3390/s19143216.
- M. Jin et al., "A Survey on Graph Neural Networks for Time Series: Forecasting, Classification, Imputation, and Anomaly Detection," p. arXiv:2307.03759doi: 10.48550/arXiv.2307.03759.
- Jing, T., Zheng, P., Xia, L., & Liu, T. (2022). Transformer-based hierarchical latent space VAE for interpretable remaining useful life prediction. *Advanced Engineering Informatics*, 54, Article 101781. <https://doi.org/10.1016/j.aei.2022.101781>
- Kipf, T. N., & Welling, M. (2016). Semi-Supervised Classification with Graph Convolutional Networks. *International Conference on Learning Representations*.
- G. A. Landis, S. G. Bailey, and R. Tischler, "Causes of Power-Related Satellite Failures," in *2006 IEEE 4th World Conference on Photovoltaic Energy Conference*, 7-12 May 2006 2006, vol. 2, pp. 1943–1945, doi: 10.1109/WCPEC.2006.279878.
- León-López, K. M., Mouret, F., Arguello, H., & Tourneret, J. Y. (2022). Anomaly detection and classification in multispectral time series based on hidden Markov models. *IEEE Transactions on Geoscience and Remote Sensing*, 60, 1–11. <https://doi.org/10.1109/TGRS.2021.3101127>
- Li, D., Chen, D., Jin, B., Shi, L., Goh, J., & Ng, S.-K. (2019). MAD-GAN: Multivariate Anomaly Detection for Time Series Data with Generative Adversarial Networks. In I. V. Cham, V. Tetko, P. K. Kürková, & F. Theis (Eds.), *Artificial Neural Networks and Machine Learning – ICANN 2019: Text and Time Series* (pp. 703–716). Springer International Publishing.
- Li, Z., Yu, J., Zhang, G., & Xu, L. (2023). Dynamic spatio-temporal graph network with adaptive propagation mechanism for multivariate time series forecasting. *Expert Systems with Applications*, 216, Article 119374. <https://doi.org/10.1016/j.eswa.2022.119374>
- F. T. Liu, K. M. Ting, and Z. H. Zhou, "Isolation Forest," in *2008 Eighth IEEE International Conference on Data Mining*, 15–19 Dec. 2008 2008, pp. 413–422, doi: 10.1109/ICDM.2008.17.
- Liu, D., Pang, J., Song, G., Xie, W., Peng, Y., & Peng, X. (2017). Fragment anomaly detection with prediction and statistical analysis for satellite telemetry. *IEEE Access*, 5, 19269–19281. <https://doi.org/10.1109/ACCESS.2017.2754447>
- Lu, Y., Shao, Q., Yue, H., & Yang, F. (2019). A Review of the Space Environment Effects on Spacecraft in Different Orbits. *IEEE Access*, 7, 93473–93488. <https://doi.org/10.1109/ACCESS.2019.2927811>
- T. Nakamura, M. Imamura, R. Mercer, and E. Keogh, "MERLIN: Parameter-Free Discovery of Arbitrary Length Anomalies in Massive Time Series Archives," in *2020 IEEE International Conference on Data Mining (ICDM)*, 17–20 Nov. 2020 2020, pp. 1190–1195, doi: 10.1109/ICDM50108.2020.00147.
- Nalepa, J., Myller, M., Andrzejewski, J., Benecki, P., Piechaczek, S., & Kostrzewska, D. (2022). Evaluating algorithms for anomaly detection in satellite telemetry data. *Acta Astronautica*, 198, 689–701. <https://doi.org/10.1016/j.actaastro.2022.06.026>
- J. Pang, D. Liu, Y. Peng, and X. Peng, "Collective Anomalies Detection for Sensing Series of Spacecraft Telemetry with the Fusion of Probability Prediction and Markov Chain Model," *Sensors*, vol. 19, no. 3, doi: 10.3390/s19030722.
- O. Parisot, P. Pinheiro, and P. Hitzelberger, "Designing IoT architectures: Learning from Massive Spacecraft Telemetry Data Analytics," *ERCIM News*, vol. 2019, no. 119, / 2019. [Online]. Available: <https://ercim-news.ercim.eu/en119/special/designing-iot-architectures-learning-from-massive-spacecraft-telemetry-data-analytics>.
- Park, D., Hoshi, Y., & Kemp, C. C. (2018). A Multimodal Anomaly Detector for Robot-Assisted Feeding Using an LSTM-Based Variational Autoencoder. *IEEE Robotics and Automation Letters*, 3(3), 1544–1551. <https://doi.org/10.1109/LRA.2018.2801475>
- Peng, X., Pang, J., Peng, Y., & Liu, D. (2016). Review on anomaly detection of spacecraft telemetry data. *Chinese Journal of Scientific Instrument*, 37(9), 1929–1945.
- Pilastré, B., Boussoff, L., D'Escrivan, S., & Tourneret, J.-Y. (2020). Anomaly detection in mixed telemetry data using a sparse representation and dictionary learning. *Signal Processing*, 168, Article 107320. <https://doi.org/10.1016/j.sigpro.2019.107320>
- Ruff, L., et al. (2018). Deep One-Class Classification. *Presented at the Proceedings of the 35th International Conference on Machine Learning, Proceedings of Machine Learning Research*.
- M. Sakurada and T. Yairi, "Anomaly Detection Using Autoencoders with Nonlinear Dimensionality Reduction," presented at the Proceedings of the MLSDA 2014 2nd Workshop on Machine Learning for Sensory Data Analysis, Gold Coast, Australia QLD, Australia, 2014. [Online]. Available: <https://doi.org/10.1145/2689746.2689747>.
- Shang, Z., Zhao, Z., Yan, R., & Chen, X. (2023). Core loss: Mining core samples efficiently for robust machine anomaly detection against data pollution. *Mechanical Systems and Signal Processing*, 189, Article 110046. <https://doi.org/10.1016/j.ymssp.2022.110046>
- Y. Shin et al., "ITAD: Integrative Tensor-based Anomaly Detection System for Reducing False Positives of Satellite Systems," presented at the Proceedings of the 29th ACM International Conference on Information & Knowledge Management, Virtual Event, Ireland, 2020. [Online]. Available: <https://doi.org/10.1145/3340531.3412716>.
- Y. Song, J. Yu, D. Tang, J. Yang, L. Kong, and X. Li, "Anomaly Detection in Spacecraft Telemetry Data using Graph Convolution Networks," in *2022 IEEE International Instrumentation and Measurement Technology Conference (I2MTC)*, 16–19 May 2022 2022, pp. 1–6, doi: 10.1109/I2MTC48687.2022.9806645.
- Y. Su, Y. Zhao, C. Niu, R. Liu, W. Sun, and D. Pei, "Robust Anomaly Detection for Multivariate Time Series through Stochastic Recurrent Neural Network," presented at the Proceedings of the 25th ACM SIGKDD International Conference on Knowledge Discovery & Data Mining, Anchorage, AK, USA, 2019. [Online]. Available: <https://doi.org/10.1145/3292500.3330672>.
- Suo, M., Tao, L., Zhu, B., Chen, Y., Lu, C., & Ding, Y. (2020). Soft decision-making based on decision-theoretic rough set and Takagi-Sugeno fuzzy model with application to the autonomous fault diagnosis of satellite power system. *Aerospace Science and Technology*, 106, Article 106108. <https://doi.org/10.1016/j.ast.2020.106108>
- J. Tang, J. Li, Z. Gao, and J. Li, "Rethinking Graph Neural Networks for Anomaly Detection," presented at the Proceedings of the 39th International Conference on Machine Learning, Proceedings of Machine Learning Research, 2022. [Online]. Available: <https://proceedings.mlr.press/v162/tang22b.html>.
- S. Tariq et al., "Detecting Anomalies in Space using Multivariate Convolutional LSTM with Mixtures of Probabilistic PCA," presented at the Proceedings of the 25th ACM SIGKDD International Conference on Knowledge Discovery & Data Mining, Anchorage, AK, USA, 2019. [Online]. Available: <https://doi.org/10.1145/3292500.3330776>.
- Tax, D. M. J., & Duin, R. P. W. (2004). Support Vector Data Description. *Machine Learning*, 54(1), 45–66. <https://doi.org/10.1023/B:MACH.0000008084.60811.49>
- Veličković, P., Cucurull, G., Casanova, A., Romero, A., Liò, P., & Bengio, Y. (2018). Graph Attention Networks. *International Conference on Learning Representations*.
- Wang, F., et al. (2023). Inherently interpretable physics-informed neural network for battery modeling and prognosis. *IEEE Transactions on Neural Networks and Learning Systems*, 1–15. <https://doi.org/10.1109/TNNLS.2023.3329368>

- Y. Wang, Y. Wu, Q. Yang, and J. Zhang, "Anomaly Detection of Spacecraft Telemetry Data Using Temporal Convolution Network," in *2021 IEEE International Instrumentation and Measurement Technology Conference (I2MTC)*, 17-20 May 2021 2021, pp. 1-5, doi: 10.1109/I2MTC50364.2021.9459840.
- J. Wang, H. Li, L. Wang, and Z. Xu, "Satellite Telemetry Data Anomaly Detection using Multiple Factors and Co-Attention based LSTM," in *2023 IEEE Wireless Communications and Networking Conference (WCNC)*, 26-29 March 2023 2023, pp. 1-6, doi: 10.1109/WCNC55385.2023.10118903.
- Wang, F., Zhao, Z., Ren, J., Zhai, Z., Wang, S., & Chen, X. (2022). A transferable lithium-ion battery remaining useful life prediction method from cycle-consistency of degradation trend. *Journal of Power Sources*, 521, Article 230975. <https://doi.org/10.1016/j.jpowsour.2022.230975>
- Wang, F., Zhao, Z., Zhai, Z., Shang, Z., Yan, R., & Chen, X. (2023/04/01/ 2023.). Explainability-driven model improvement for SOH estimation of lithium-ion battery. *Reliability Engineering & System Safety*, 232, Article 109046. <https://doi.org/10.1016/j.ress.2022.109046>
- Wu, J., Yao, L., Liu, B., Ding, Z., & Zhang, L. (2020). Combining OC-SVMs With LSTM for detecting anomalies in telemetry data with irregular intervals. *IEEE Access*, 8, 106648-106659. <https://doi.org/10.1109/ACCESS.2020.3000859>
- Xie, L., Pi, D., Zhang, X., Chen, J., Luo, Y., & Yu, W. (2021). Graph neural network approach for anomaly detection. *Measurement*, 180, Article 109546. <https://doi.org/10.1016/j.measurement.2021.109546>
- T. Yairi, Y. Fukushima, C. F. Liew, Y. Sakai, and Y. Yamaguchi, "A Data-Driven Approach to Anomaly Detection and Health Monitoring for Artificial Satellites," in *Advances in Condition Monitoring and Structural Health Monitoring*, Singapore, L. Gelman, N. Martin, A. A. Malcolm, and C. K. Liew, Eds., 2021// 2021: Springer Singapore, pp. 129-141.
- Yairi, T., Takeishi, N., Oda, T., Nakajima, Y., Nishimura, N., & Takata, N. (2017). A data-driven health monitoring method for satellite housekeeping data based on probabilistic clustering and dimensionality reduction. *IEEE Transactions on Aerospace and Electronic Systems*, 53(3), 1384–1401. <https://doi.org/10.1109/TAES.2017.2671247>
- Yang, L., Ma, Y., Zeng, F., Peng, X., & Liu, D. (2021). Improved deep learning based telemetry data anomaly detection to enhance spacecraft operation reliability. *Microelectronics Reliability*, 126, Article 114311. <https://doi.org/10.1016/j.microrel.2021.114311>
- Yoon, J., Jordon, J., & Schaar, M. (2018). GAIN: Missing Data Imputation using Generative Adversarial Nets. *Presented at the Proceedings of the 35th International Conference on Machine Learning, Proceedings of Machine Learning Research*.
- Yu, J., Song, Y., Tang, D., Han, D., & Dai, J. (2021). Telemetry Data-Based Spacecraft Anomaly Detection With Spatial-Temporal Generative Adversarial Networks. *IEEE Transactions on Instrumentation and Measurement*, 70, 1–9. <https://doi.org/10.1109/TIM.2021.3073442>
- Yu, B., Yin, H., & Zhu, Z. (2018). Spatio-temporal graph convolutional networks: a deep learning framework for traffic forecasting. *Presented at the Proceedings of the 27th International Joint Conference on Artificial Intelligence, Stockholm, Sweden*.
- Zeng, Z., Jin, G., Xu, C., Chen, S., Zeng, Z., & Zhang, L. (2022). Satellite Telemetry Data Anomaly Detection Using Causal Network and Feature-Attention-Based LSTM. *IEEE Transactions on Instrumentation and Measurement*, 71, 1–21. <https://doi.org/10.1109/TIM.2022.3151930>
- Zhao, Z., Wu, J., Li, T., Sun, C., Yan, R., & Chen, X. (2021). Challenges and opportunities of AI-enabled monitoring, diagnosis & prognosis: a review. *Chinese Journal of Mechanical Engineering*, 34(1), 56. <https://doi.org/10.1186/s10033-021-00570-7>
- H. Zhao et al., "Multivariate Time-Series Anomaly Detection via Graph Attention Network," in *2020 IEEE International Conference on Data Mining (ICDM)*, 17-20 Nov. 2020 2020, pp. 841-850, doi: 10.1109/ICDM50108.2020.00093.
- Zhou, J., et al. (2020). Graph neural networks: A review of methods and applications. *AI Open*, 1, 57–81. <https://doi.org/10.1016/j.aiopen.2021.01.001>
- B. Zong et al., "Deep autoencoding gaussian mixture model for unsupervised anomaly detection," in *International conference on learning representations*.